HHS Public Access

Author manuscript

J Immunol. Author manuscript; available in PMC 2019 January 01.

Published in final edited form as:

J Immunol. 2018 January 01; 200(1): 316–326. doi:10.4049/jimmunol.1602017.

Modulation of the Alternative Pathway of Complement by Murine Factor H-Related Proteins

Alexandra H. Antonioli[*], **Janice White**[†], **Frances Crawford**[†], **Brandon Renner**[*], **Kevin J. Marchbank**[§], **Jonathan P. Hannan**[*], **Joshua M. Thurman**[*], **Philippa Marrack**[‡], and **V. Michael Holers**[*]

[*]Department of Medicine, University of Colorado School of Medicine, Aurora, CO

[†]Howard Hughes Medical Institute, Denver, CO 80206

[‡]Howard Hughes Medical Institute, Denver, CO 80206; Department of Biomedical Research, National Jewish Health, Denver, CO 80206; Department of Immunology and Microbiology, University of Colorado School of Medicine, Aurora, CO 80045

[§]Institute of Cellular Medicine, Newcastle University, Newcastle-upon-Tyne, UK

Abstract

Factor H (FH) is a key alternative pathway (AP) regulator that controls complement activation both in fluid phase and on specific cell surfaces, thus allowing the innate immune response to discriminate between self and foreign pathogens. However, the interrelationships between Factor H and a group of closely related molecules, designated the Factor H-Related (FHR) proteins, are currently not well understood. While some studies have suggested that human FHR proteins possess complement regulatory abilities, recent studies have shown that FHR proteins are potent deregulators. Furthermore, the roles of the FHR proteins have not been explored in any *in vivo* models of inflammatory disease. Here we report the cloning and expression of recombinant mouse FH and three FHR proteins (FHRs A-C). Results from functional assays show that FHR-A and FHR-B proteins antagonize the protective function of FH in sheep erythrocyte hemolytic assays and increase cell-surface C3b deposition on a mouse kidney proximal tubular cell line (TEC) and a human retinal pigment epithelial cell line (ARPE-19). We also report apparent K_D values for the binding interaction of mouse C3d with mouse FH (3.85μM), FHR-A (136 nM), FHR-B (546 nM), and FHR-C (1.04 μM), which directly correlate with results from functional assays. Together our work suggests that like their human counterparts, a subset of mouse FHR proteins have an important modulatory role in complement activation. Further work is warranted to define the *in vivo* context-dependent roles of these proteins and determine whether FHRs are suitable therapeutic targets for the treatment of complement-driven diseases.

Introduction

Understanding regulatory mechanisms by which the alternative pathway (AP) controls spontaneous activation of complement in the fluid phase and the amplification of

Corresponding author: V. Michael Holers, M.D., Division of Rheumatology, B-115, 1775 Aurora Court, M20-3102-E, Aurora, CO 80045, Phone: 303-724-7605, Fax: 303-724-7581, Michael.Holers@ucdenver.edu.

complement on specific surfaces has important implications for treating complement-driven inflammatory disease. Unlike the classical (CP) or lectin (LP) pathways, the AP does not require any specific molecular recognition for its initiation but is activated by hydrolysis of C3 to C3(H_2O) in the fluid phase, which results in activation and production of C3b through the activities of Factor D, Factor B and Properdin. This phenomenon, known as C3 tick-over, occurs spontaneously and allows for the rapid initiation and amplification of complement. Given that this pathway is responsible for ≥80% of the final downstream effect of initial specific activation of the CP and LP, precise control of the AP and its amplification loop is required (1).

Factor H (FH) is a major soluble complement regulator that is essential for controlling AP activation in the fluid phase and on cell surfaces. Several human diseases are associated with mutations and autoantibodies that alter either FH function, or the activities of the closely related FH related proteins (FHRs). For example, mutations or polymorphisms in the *CFH* and *CFHR* gene family have been linked to the renal diseases atypical hemolytic uremic syndrome (aHUS) and IgA nephropathy as well as diseases that have glomerular pathologies including dense deposit disease (DDD) and FHR5 nephropathy, which are encompassed under the C3 glomerulopathy (C3G) umbrella (2–4). Other autoimmune diseases associated with alterations within the *CFH* and *CFHR* gene family include systemic lupus erythematosus (SLE) and age-related macular degeneration (AMD) (5–7).

Given the recent expansion in research towards understanding the human FHR protein family member disease associations, one question that remains unanswered is whether the mouse FHR proteins are functional orthologs to their human counterparts. The mouse FH (mFH) gene consists of 22 exons which share 63% homology with human *CFH* and encode a protein composed of 20 short consensus repeat (SCRs) domains (8). Unlike its human counterpart, the *mFH* gene does not have a FHL-1 variant, although it does contain an unspliced exon (exon 9) that could encode a SCR domain with a stop codon. Like their human FHR counterparts, a total of five mouse FHR (mFHR) genes have been identified, and evidence for four mFHR proteins have been inferred from mRNA transcripts isolated from a mouse liver cDNA library; however, direct comparison to the human *CFHR* gene family is not straightforward (9, 10). These predicted mouse proteins also exhibit high sequence identity with important ligand binding and self-surface recognition domains of mouse FH. After the initial characterization of the four classes of mFHR transcripts by Vik et al. 1990 (9), this gene family was not thoroughly examined until Hellwage and colleagues published data on mFHR protein expression and binding partners (10). However, little subsequent work has been published which characterizes these genes, evaluates the functional roles of the proteins they encode, or examines the concentrations and functions of these proteins *in vivo*.

One potential limitation to studying the mouse *FHR* gene family lies with understanding the published nomenclature as it relates to that of the human *FHR* gene family. While the nomenclature for the mouse *FHR* genes (labeling them alphabetically as A, B, C based on their position from mFH) was proposed over a decade ago, a current search of genome browsers lists these genes under various aliases including *CFHR4/2*, *CHFR2*, *FHR-1* or *FHR-3* (10). For example, the mouse gene referred to as *CFHR-1* is located at the *mFHR-E*

gene position which is furthest from the mouse factor H gene. This same gene was originally classified by Vik and colleagues as clone 13G1 and is a “class D” mFHR transcript (9). Additionally, the mouse genes are predicted to have higher sequence identity to both full-length factor H and to one another compared to the human FHR genes. Therefore, given our relative lack of knowledge about the potential functions of the mouse FHR proteins, we elected to investigate three constructs that were discussed in the two original publications on mouse FHRs. We generated a mFHR-A construct based on the original prototype sequence provided by Vik et al. 1990 (9), and the sequences of mFHR-B and mFHR-C constructs were generated based on work by Hellwage and colleagues (10). Notably, all three of the murine constructs that were chosen for this study lack a dimerization domain found in human FHR-1, FHR-2, and FHR-5 (11). However other sequences may mediate dimerization of the murine FHRs, and therefore we chose to focus our efforts on obtaining a better understanding of mouse FHR protein function.

We hypothesized that mFHRs, like their human counterparts, regulate complement activation by antagonizing FH function. To test this hypothesis, a comprehensive characterization of the mFHR proteins was undertaken. Hemolytic assays were used to assess the function of recombinant proteins. To characterize the interaction between mFHRs and C3b/C3d fragments, a combination of ELISA and surface plasmon resonance experiments were performed. To elucidate the functional homology between a conserved C3d binding site on the human and mouse FHR proteins, mutant mFHRs were generated and their activity was assessed. Using *in vitro* experiments with two cell lines, the role of mFHRs on complement regulation on different cell surfaces was evaluated. In sum, these analyses provide a better understanding of a subset of mouse FHR orthologs and provide a potential means to modulate FHR function in an informative manner *in vivo* and better understand how manipulation of their activities can potentially ameliorate the human diseases to which these proteins contribute in a pathophysiologically important manner.

Materials and Methods

Sequence analysis

DNA and protein sequences for the human and mouse FH and mFHR families and C3b/C3d proteins were analyzed using the Bioinformatics Resource Portal (ExPASy) of the Swiss Institute of Bioinformatics (https://www.expasy.org), the Ensembl database which is a joint project between the European Bioinformatics Institute and the Wellcome Trust Sanger Institute (http://www.ensembl.org), and the UCSC Genome Browser hosted by the University of California, Santa Cruz (https://genome.ucsc.edu).

Mouse FH and FHR protein expression

DNA sequences of full-length mFH and mFHR constructs including mFHR-A (based on the sequence for class A clone 3A4/5G4 by Vik et al. 1990 (9)), mFHR-B, mFHR-C, and mFH19–20 were generated commercially (GeneArt® by Life Technologies). The unique Uniprot identifiers (ID) for each construct include: mFH (Uniprot: P06909), mFHR-A (Uniprot: Q61407), mFHR-B (Uniprot: Q4LDF6), mFHR-C (Uniprot: Q0KHD3), and mFH19–20 (Uniprot: P06909 residues 1112–1234). Each DNA sequence was codon-

optimized (*Homo sapiens*) and engineered into a Gateway® pDONR221 entry vector (Life Technologies) following previously published construct design and experimental conditions (12). For protein expression, Freestyle™ 293-F cells (Invitrogen) were obtained and subcultured in Freestyle™ 293 Expression Medium every three days. Transfections were performed using FreeStyle™ MAX Reagent (Life Technologies) according to manufacturer's instructions. Cell supernatant was harvested 5–7 days post-transfection using centrifugation at 8,000 rpm for 15 min in sterile 250 ml tubes.

Mutant mouse FHR constructs

To create mutant mFHR constructs, a Quick Change Lightning Site Directed Mutagenesis Kit (Agilent Technologies, Santa Clara, CA) was used according to manufacturer's directions. Generation of a N340A/D342A mFHR-A mutant was created with the following primers that were codon-optimized for mammalian cell expression: forward 5′-cct atc gac gcc ggg gct atc acc agc ctg-3′ and reverse 3′-gga tag ctg cgg ccc cga tag tgg tcg gac -5′ to create the following sequence: PIDAGAITSL. The mutant N220A/D222A mFHR-B construct was created with primers: forward 5′-ccc atc gac gct ggg gct atc acc agc ctg-3′ and reverse 3′-ggg tag ctg cga ccg cga tag tgg tcg gac-5′ to create the following sequence: PIDAGAITSL.

FH and FHR protein purification

Purification of the FH and FHR proteins was performed using immobilized metal affinity chromatography (IMAC). Harvested supernatant was diluted with 5X buffer (0.1 M sodium phosphate pH 7.8, 0.1 M imidazole, and 2.5 M NaCl). Samples were applied to either a 5-ml HisTrap HP column (GE Healthcare Life Sciences) or column containing HisPur™ Ni-NTA Resin (Thermo Fisher Scientific) as per manufacturer's instructions. After applying supernatant to the Ni-NTA column, bound His-tagged proteins were eluted using a linear imidazole gradient from 20 mM and 0.5 M imidazole. Most proteins were completely eluted from the resin using 0.2 M imidazole; however, 1–2 ml fractions were collected and analyzed by monitoring the OD ratio at 260/280. Protein purity was assessed by SDS-PAGE. Fractions containing purified protein were pooled and concentrated at RT using a Vivaspin 20 spin concentrator (Millipore Inc.). Proteins were buffer exchanged into Dulbecco's Phosphate Buffered Saline (DPBS: 2.7 mM KCl, 1.5 mM KH_2PO_4, 138 mM NaCl, 8.1 mM Na_2PO_4, pH 7.4). A polishing step was performed by applying protein to either S200 or S300 HiPrep 16/60 Sephacryl size exclusion columns (GE Healthcare) on an ÄKTAPure high pressure liquid chromatography system (GE Healthcare) which had been equilibrated with DPBS. Peak fractions were eluted in 1 ml volumes and analyzed by SDS-PAGE. Protein concentrations were determined using a NanoDrop Spectrophotometer (Thermo Fisher Scientific) by entering molecular weight (MW) values and molar extinction coefficients for each protein. Purified proteins were flash frozen in 50–100 μL aliquots using liquid nitrogen and stored at -80°C. SDS-PAGE analysis was used to analyze protein purity for both glycosylated and deglycosylated proteins. To deglycosylate proteins, a Remove-iT® PNGase F and a Magnetic Chitin Bead Protocol was used according to manufacturer's instructions (New England Biolabs).

Mouse C3d expression and purification

A construct encoding wild-type mouse C3d in a pCR Topo vector was obtained from a previous laboratory stock. This construct was sequenced with M13 forward and reverse primers to confirm that the DNA sequence could be translated to match the following Uniprot ID: P01027 (residues 1002–1303). The thioester-containing domain (TED) of C3b is contained within this sequence. Four residues in this sequence (Cys-Gly-Glu-Gln) make up a fifteen member thiolactone ring which facilitates the covalent interaction between C3b and cell surfaces through residue Q1013. Primers were used to mutate C1010A to prevent dimerization and reactivity of C3d by mutating the sequence from PAG**C**GEQN to PAG**A**GEQN as previously described (13). Primers (forward: 5′-ccc gca ggc gct ggg gaa cag aac - 3′ and reverse: 3′-gtt ctg ttc ccc agc gcc tgc ggg-5′) and the Quick Change Lightning Site Directed Mutagenesis Kit were used (Agilent Technologies) followed by transformation of X10-Gold Ultracompetent cells (Stratagene). Subcloning of the mC3D construct into a pGEX-2T GST expression vector (GE Healthcare Life Sciences) was performed. Dual digestion of both vectors was performed using BamHI-HF and EcoR1-HF restriction enzymes per manufacturer's specifications (New England Biolabs) followed by gel purification and fragment ligation using T4 DNA ligase. Both pGEX forward and reverse primers were used to confirm the sequence of the mC3d-pGEX-2T GST expression construct prior to transformation and expression of protein in BL21 (DE3) cells.

Circular Dichroism (CD) spectroscopy

Recombinant mC3d was analyzed using CD spectroscopy. A Jasco J-815 spectropolarimeter (Jasco, Inc., Easton, MD) with a Jasco DP-500/PS2 system was used in this experiment. A Lauda model RMS circulating water bath (LAUDA-Brinkman, Delran, NJ) was used to maintain temperature control of the optical cell. Results are expressed as mean molar ellipticity [θ] (deg·cm^2·dmol^{-1}) and were calculated using the following equation:

$$[\theta]=[\theta obs \cdot MRW/10lc]$$

where θ_{obs} is the observed ellipticity in millidegrees, MRW is the mean residue weight of the peptide (peptide molecular weight/number of residues), l is the optical path length of the cell in centimeters, and c is the peptide concentration in mg/ml. A solution of 1 mg/ml mC3d in PBS was used in this experiment. Variable wavelength measurements of peptide solutions were scanned at 5°C from 195 nm to 250 nm, in 0.5 nm increments at a scan rate of 50 nm per minute.

Differential scanning fluorimetry

The thermal stability profiles of mFH, mFHR, and C3d recombinant proteins were investigated by combining 75 μg/ml of protein in PBS (Corning, catalog: 21-040-CV) and dye in a total reaction volume of 30 μl. A fresh 300X stock of SYPRO Orange (5,000X) was diluted in fresh DMSO (Sigma-Aldrich) and a final concentration of 10X SYPRO Orange per reaction was used. This specific dye has excitation/emission wavelength profiles of 490 nm and 575 nm. Experiments were performed in a 96-well PCR plate (Bio-Rad) which was sealed using Optical-Quality Sealing Tape (Bio-Rad). An iQ5 Real-time PCR Detection

instrument heated samples at 1°C/min from 20°C to 95°C with a fluorescence reading recorded every 0.2°C. The melting point (T_m) for each of the proteins was determined by fitting data to a Boltzmann model and data were normalized in GraphPad in order to make comparisons between different proteins (14).

Enzyme-Linked Immunosorbent Assay (ELISA) with mouse C3d

To examine the interaction between mC3d and mFH/mFHR proteins, ELISA assays were used. Clear flat bottom polystyrene 96-well microplates (Corning®) were coated overnight at 4°C with 50 μl/well of recombinant mC3d at a concentration of 10 μg/ml in 50 mM sodium bicarbonate buffer (pH 8.8). Plates were washed 3 times in wash buffer (PBS + 0.05% Tween 20) before blocking with 100 μl/well PBS+ 1% BSA. Plates were again washed prior to addition of mFH or mFHR proteins. Following incubation with mFH/mFHR proteins for 1 hour at RT, plates were washed before addition of 1:1000 anti-6X His tag® antibody (Abcam, catalog: ab1187) in 100 μl PBS + 1% BSA for 1 hour at RT. Finally, plates were washed before developing with ABTS. Following a 30 min RT incubation, OD values were determined at wavelength 405 nm.

Surface plasmon resonance

A Biacore® T200 instrument (GE Healthcare Life Sciences) was used to calculate apparent K_D values for mFH and mFHR proteins and mC3d. A Series S Sensor CM5 chip (GE Healthcare Life Sciences) was chemically coupled with 2500 response units (RU) of mC3d in 10 mM Acetate buffer pH 4.0 using standard amine coupling techniques. To assess binding with mC3d, mFH and mFHR wild-type and mutant proteins were serially diluted in HBS-EP+ buffer (10mM HEPES pH 7.4, 150mM NaCl, 3mM EDTA and 0.005% v/v Surfactant P20) and injected at a flow rate of 15 μl/ml for ~80 s while dissociation of mC3d:mFH/mFHR complexes was monitored to 600 s after injection. The running buffer was HBS-EP+. Guided by the Biacore® evaluation software a two-state reaction model was determined to provide the best fit and therefore this model was used to estimate the K_D values presented herein.

Erythrocyte hemolytic assays

The functional activities of mFH and mFHR proteins were analyzed using erythrocyte hemolytic assays which have been previously described (15). Sheep erythrocytes (Complement Technology Inc.) were obtained and resuspended in MgEGTA buffer (0.1 M $MgCl_2$, 0.1 M EGTA pH 7.3). To each 24 μl reaction, ~$0.7–1 \times 10^6$ cells (in MgEGTA buffer) were added to the bottom of a PCR tube. Either mFH or mFHR proteins were added to the cells followed by normal mouse serum (NMS) from C57BL/6 mice (40% final concentration). Reactions were incubated at 37°C for 30 min and quenched using 200 μl gelatin veronal buffer (GVB) buffer containing EDTA. Following centrifugation, 180 μl was read at OD_{412}. As a negative control, the same reaction mixture was prepared using cells and normal mouse serum in PBS without recombinant protein. The percentage of hemolysis was determined by subtracting the OD_{412} of the background hemolysis control (PBS + NMS) and dividing by the maximum hemolysis of cells in sterile water.

Competition assays

Erythrocyte hemolytic competition assays were performed to evaluate the competition between mFH and the mFHRs. For these reactions, 2μM of recombinant mouse FH was added to 1×10^6 sheep erythrocytes in a 24 μL reaction volume with 20% normal mouse serum. mFH was added to the cells five minutes prior to adding the 20% normal mouse serum and either 1μM mFHR-A or 4μM mFHR-B to the samples. Samples were then incubated at 37°C for 30 min and quenched using 200 μl gelatin veronal buffer (GVB) buffer containing EDTA. Following centrifugation, 180 μl was read at OD_{412}. The data represent means ± SEM from at least three separate experiments with three replicates per sample.

Flow cytometry

Murine renal tubular epithelial cells (TECs) were cultured in DMEM media supplemented with 10% FBS, 0.1g/ml penicillin/streptomycin, and 1% non-essential amino acids (Thermo Fisher Scientific). Cells were grown to 80–90% confluence prior to analysis. The cells were treated with Accutase and then washed using PBS. Cells were incubated in 10% normal mouse serum (NMS) in the presence or absence of increasing amounts of recombinant mFHR proteins for 30 min. Surface-bound C3b was determined by incubating cells with a 1:150 dilution of FITC-labeled goat anti-mouse C3 Ab (Cappel #55500) in the dark on ice for 60 min. Cells were next washed twice and resuspended in FACS buffer (1X PBS with 1% BSA). Samples were run using a FACSCalibur flow cytometer (BD Biosciences), and results were analyzed using FlowJo software. To measure C3b deposition on retinal pigment epithelial cells (ARPE-19), experiments were performed according to previously published methods (16). Briefly, ARPE-19 cells were cultured in Dulbecco's modified Eagle's medium F12 (Invitrogen) with 10% FBS, and 1X penicillin/streptomycin. Stressed cells were incubated with 1mM H_2O_2 for 1 hour in fresh media while unstressed cells were incubated in fresh media. Cells were treated with Accutase (Innovative Cell Technologies), washed, and resuspended in DPBS. Next, cells were incubated with mFHR proteins for 15 min prior to addition of 10% NMS and further incubation at 37°C for 35 min. Cell surface C3b deposition was examined by gating cells based on their forward (FSC-height) and side scatter (SSC) properties. At least 60,000 cells were analyzed and the mean fluorescence intensity (MFI) was plotted.

Results

Generation and assessment of recombinant FH and FHR proteins

The positions of the mFH and mFHR gene family were analyzed using various genome browsers prior to designing recombinant DNA constructs (Fig. 1A). To analyze the function of mFH and mFHR proteins, expression constructs for mFH, mFHR-A, mFHR-B, mFHR-C, and mFH19–20 were synthetically generated (Fig. 1B). The sequence for mFHR-A was based on the prototype transcript sequence for the class A clones (3A4/5G4) characterized by Vik and colleagues (9), while the mFH19–20 construct consisted of the last two C-terminal SCR domains of full-length mFH (15, 16). Constructs were engineered with N-terminal His_6 tags rather than C-terminal tags, as the C-terminal domains of mouse FH and FHR proteins contain putative C3b/C3d and GAG binding sites. Recombinant proteins were expressed by transient transfection of mammalian 293-F cells. This system was chosen in

order to produce proteins with glycosylation patterns closer to native protein expression patterns, which may have implications for proper protein folding and function. Additionally, we sought to produce proteins that did not require deglycosylation to produce a uniform protein population and which could be used in functional studies and *in vivo* disease models. Lastly, 293-F cell expression provided a serum-free method for expressing and purifying mFHR proteins, while preventing cross-reactivity and/or contamination from complement components and other proteins that are present in serum-based expression media.

Recombinant proteins were purified from supernatant using a combination of immobilized metal affinity chromatography and gel filtration methods. Analytical SDS-PAGE was used to examine protein purity under reducing conditions (Figs. 2A and 2B). While bands for glycosylated mFH, mFHR-A, and mFHR-C are observed near their predicted molecular weights, mFHR-B appears as a band at ~55kDa. Therefore, deglycosylation of the proteins using PNGaseF was performed. Following deglycosylation of the proteins, PNGaseF was removed from each sample before performing SDS-PAGE. When deglycosylated, all proteins run at their predicted molecular weights: mFH (~140kDa), mFHR-A (~55kDa), mFHR-B (~35–40kDa), and mFHR-C (~110kDa). In a separate experiment, PNGaseF which has a molecular weight of ~36kDa was not removed after deglycosylation of mFHR-A and mFHR-B and can be seen as a band running beneath both mFHR-A and mFHR-B (Fig. 2B). Differential scanning fluorimetry (DSF) was used to assess the quality of the folded proteins and analyze their stability in PBS. This technique proved to be an effective method for analyzing the quality of batches of protein produced from different transfections. DSF also allowed for a way to examine protein stability in different buffer conditions. Normalized results from DSF show that mFH and mFHR proteins exhibit denaturation curves with melting points (T_m) ~60–65°C in PBS suggesting that the recombinant proteins are properly folded (Fig. 2C).

Mouse FHR-A and FHR-B are potent antagonists of mouse FH on sheep erythrocytes

Previous research has shown that the C-terminal end of human Factor H plays a critical role in the regulation of complement on cell surfaces (15). The C-terminal SCR domains of FH (SCRs19–20) can discriminate between host and non-host surfaces. In sheep erythrocyte hemolytic assays, lysis of normal sheep red blood cells occurs in the presence of the recombinant FH19–20 inhibitor while fluid phase complement activation remains unaffected. Both FH and the FH19–20 inhibitor have ~7-fold higher affinity for surfaces coated with C3b and high amounts of sialic acid (15). Additionally, competition assays showed that FH19–20 inhibits FH-mediated control of alternative pathway driven complement lysis on host-like polyanion-bearing cells.

To investigate the effects that mouse FHR proteins exhibit on FH protection of host-like surfaces, hemolytic assays using normal sheep red blood cells (SRBCs) were performed. As a positive control for deregulation of FH function, mouse FH19–20 was designed and expressed using methods described. Normal sheep erythrocytes were incubated for 30 minutes at 37°C with complement sufficient WT mouse serum (40%) and increasing concentrations of mFHR-A, mFHR-B, mFHR-C, mFH, and mFH 19–20 (Fig. 3). In agreement with previous studies we found that mFH19–20 activates complement by

inhibiting FH protection of SRBCs (15, 17). Interestingly, both mFHR-A and mFHR-B appear to be more potent antagonists of mFH in this assay (Fig. 3A). Thus, complete hemolysis was observed with addition of ~4 μM mFHR-A, while two-fold higher concentrations of mFHR-B were required to induce just over 50% lysis of erythrocytes. In contrast, 5 μM mFH19–20 inhibited mFH cell-surface protection of the erythrocytes by only 25%. Interestingly, mFHR-C did not antagonize mFH function on these cell surfaces. Even in the presence of high concentrations of mFHR-C (20 μM), no erythrocyte hemolysis was observed (Fig. 3B). Furthermore, competition assays were performed using mFH to demonstrate that incubation of sheep red blood cells with mFH prior to addition of mFHR-A or mFHR-B prevents hemolysis of cells (Fig. 3C).

Mouse FH and FHR proteins bind mouse C3d and mutant FHR proteins are inactive

To explore the molecular mechanism underlying the different hemolytic activities observed with the mFHR proteins, we next investigated how mFH and mFHRs engage the complement component, C3d, an analog of the thioester containing domain in C3b. Complement regulation by factor H requires binding to C3b/C3d, and we hypothesized that differential binding by the mFHRs to C3b/C3d may modulate alternative pathway activity. Previous work with mFHR-B produced in *P. pastoris* provided the first evidence that mouse FHRs interact with human C3b (10). However, differences between human and mouse C3b exist; therefore, recombinant mouse C3d was produced. Human C3d produced in our laboratory was also available in these studies for comparison. Recombinant production of human and mouse C3d using *E. coli* was performed followed by purification of the proteins using a GST-column and size exclusion chromatography. SDS-PAGE separation showed a product at approximately ~35kDa, which is the predicted molecular weight for mC3d (Supplemental Fig. 1A). Analysis of the mC3d secondary structure was performed using circular dichroism (CD). The CD spectrum revealed an alpha helical confirmation for mC3d, a result that is in agreement with the x-ray crystallography structure of human C3d (Supplemental Fig. 1B) (18). Additionally, thermal shift assays for mC3d and hC3d were performed, and the apparent T_m for mC3d (>40°C) was estimated to be slightly higher than that for hC3d (<40°C) (Supplemental Fig. 1C).

To investigate mC3d binding to mouse FH and mFHRs, ELISA assays were performed. Microtiter plates were coated with C3d and binding of mFH, mFHR-A, and mFHR-B proteins was observed (Fig. 4B). Cross-species reactivity between human C3d and mFH and mFHR proteins was also observed (Supplemental Fig. 2). To further explore this interaction, mutant constructs were made. Four key residues within human FH SCR 19 and one residue within SCR 20 have side chains that form intermolecular hydrogen bonds with C3d. All five of these key residues are conserved within the mouse FH and FHR family (Fig. 4A). Several other residues that are also important for the hFH19–20:C3d interface are indicated. To test this interaction, mutations were made to residues corresponding to human factor H residues N1117 (N1117A) and D1119 (D1119A) produce mutant mFHR-A and mutant mFHR-B proteins. No binding was observed between mC3d and mutant mFHR-A or mutant mFHR-B by ELISA (Fig. 4B).

Binding affinities of mFHR proteins and mC3d directly correlate with their functional activities

Earlier studies have analyzed the interaction between mouse FH and C3b using surface plasmon resonance (SPR). The binding of full-length mFH, and truncated versions of mFH including mFH SCRs1–5 and mFH SCRs 18–20 to both mouse and human C3b has been demonstrated (19). However, the apparent K_D values for this interaction have not been determined, and the interaction between mouse FH (and the mouse FHRs) and mC3d has not been evaluated.

Using previously described conditions for SPR experiments with mFH and C3b, binding of mFH and mFHR proteins to mC3d was investigated. We used standard amine coupling of approximately ~2500 resonance units (RU) of mC3d onto a CM5 sensor chip. Serial dilutions of mFH, mFHR-A, mFHR-B, mFHR-C, and mFH 19–20 proteins were made, and sensorgrams generated from the different dilutions were analyzed using BIA evaluation software. Data were fitted using a two-state reaction model, and apparent K_D values for each of the proteins were calculated and compared.

Apparent binding affinities varied among the different proteins. The highest binding affinities were observed for mFHR-A (K_D= 136 nM) and mFHR-B (K_D= 546 nM). These affinities were ~8-fold and ~2-fold greater than the apparent binding affinity of mFHR-C at K_D= 1.04 μM. The weakest binding affinities were observed for mFH (K_D= 3.85 μM) and the recombinant mFH 19–20 inhibitor (K_D= 22μM) (Fig. 5A and 5D). No binding interaction was observed for Mutant mFHR-A and mFHR-B proteins (containing the N1117A and D1119A pair mutation). While binding of mouse FH to mouse C3b has been previously analyzed (19), affinity values were not calculated. However, two different dissociation constants have been calculated using SPR for the interaction between human C3d and FH19–20. Kajander et al. 2011 calculated a K_D value of 0.18 μM for the C3d:FH19–20 interaction while Morgan et al. 2011 determined a K_D value between 6.2–8.2 μM (13, 20).

Mutant mouse FHR-B exhibits loss of function in hemolytic assays

To assess the function of the mutant mFHR-B protein compared with wild-type protein, a sheep erythrocyte hemolytic assay was performed using previously described methods and conditions. Results show that mutation of two out of five major putative binding residues (corresponding to human FH residues N1117A and D1119A) that form intermolecular hydrogen bonds with C3d sufficiently abrogates the ability of mFHR-B to inhibit mFH resulting in diminished hemolysis of erythrocytes (Fig. 6). At a concentration of 2 μM mFHR-B, ~20% hemolysis of sheep erythrocytes is observed, while at 8 μM mFHR-B, over 60% lysis occurs. We observe negligible hemolysis at Mutant mFHR-B concentrations of 2 μM, 4 μM, and 8 μM. These results are in good agreement with our hypothesis that the alternative pathway is modulated by mFHR proteins through their direct engagement and competition with mFH for binding to C3d and the TED domain.

Mouse FHRs activate complement on different cell surfaces

We also explored whether mFHR proteins can impair mFH function on different cell surfaces. Murine renal tubular epithelial cells (TEC) have been shown to express the membrane-bound regulator Crry on their basolateral surface while factor H regulates complement activation on their apical surface (21). TECs are targets of complement-mediated damage *in* vivo due to dysregulation and excessive activation of the alternative pathway (22). Complement activation *in vitro* occurs during the incubation of cells with 10% wild-type mouse serum and can be monitored by evaluating C3b deposition on the surface of TECs using flow cytometry. In a separate study, a FH binding partner, annexin 2 (A2), impaired complement regulation by FH and increased complement activation on TEC cells. The effect of A2 on C3b deposition was reversed by the addition of recombinant FH, but not addition of the inhibitor FH19–20 (17). Here we probed the ability of murine FHR proteins to act as antagonists of FH function on TEC cells by incubating the cells with mFHR-A or mFHR-B proteins in the presence of 10% normal mouse serum. As anticipated, both mFHR-A and mFHR-B act as potent antagonists of mFH, increasing complement activation on TEC surfaces as indicated by the increase in C3b deposition (Fig. 7).

Given the association with FHR proteins and AMD, the ability of the murine FHRs to enhance complement activation on a human retinal pigment epithelial cell line (ARPE-19) was explored. Research by Thurman and colleagues has described a mechanism by which immortalized ARPE-19 cells regulate complement activation on their surfaces. Using similar assays as described in the TEC experiments, they report that treatment of ARPE-19 cells with H_2O_2 to induce oxidative cell stress resulted in decreased surface expression of CD55 and CD59 and impaired FH cell-surface control (16). Here we used flow cytometry to examine the degree of C3b deposition on both unstressed and stressed ARPE-19 cells incubated with either mFHR-A or mFHR-B in the presence of 10% normal mouse serum. Addition of mFHR-A or mFHR-B increased complement activation on both types of cells. The ability of mFHR-A and mFHR-B to increase complement activation on healthy cells (unstressed) further supports the idea that mFHR-A and mFHR-B are potent antagonists of mFH on different nucleated cell surfaces (Fig. 8).

mFH and mFHR Antibody Production

Armenian hamsters were obtained from Cytogen Hamsters (West Roxbury, MA). Hamsters were pre-bled to obtain a stock of serum prior to immunization. On Day 0, hamsters were immunized by subcutaneous injection of 100 μg protein in Complete Freund's Adjuvant (CFA). On day 14, hamsters were boosted with 50 μg mFH/mFHR protein in Incomplete Freund's Adjuvant. On day 21, hamsters were bled and serum was tested by ELISA. Once a reasonable antibody titer was determined or after day 35, hamsters were given an intraperitoneal injection with 50 μg protein in PBS. On day 38 or later, the spleen was harvested and fused with mouse myeloma SP2/0 cells and hybridomas were screened using recombinant mFH and mFHR proteins per Kappler-Marrack protocols (https://www.nationaljewish.org/research-science/programs-depts/biomedical-research/labs/kappler-marrack-research-lab/protocols).

Discussion

The complement system is a major mediator of immune surveillance and homeostasis. At present, there is an increased focus on understanding the regulation of the different pathways, especially the AP which is the primary pathway by which the system damages cells and tissues. The spontaneous hydrolysis of C3 leading to generation of C3b must be well-controlled in order to prevent inappropriate and potentially rapid AP complement activation. Factor H is a major soluble complement regulator that is essential for controlling AP activation in plasma and on cell-surfaces through the engagement of polyanionic surface markers, such as sialic acid, and C3 fragments, such as C3b and C3d. Mutations or deletions in FH, particularly within the C-terminal region, are associated with a number of different autoimmune and inflammatory illnesses. Moreover, pathogens and altered-host cells, such as cancer cells, exploit the protective function of FH by recruiting FH to their surfaces as part of an immune evasion/modulation strategy (23–25).

While a significant amount is known about the structure and function of FH, the functional roles of a group of structurally similar molecules, designated the FHR proteins are less understood. Here we present a more extensive characterization of the mFHR-B and mFHR-C proteins in addition to evaluating a third putative FHR protein, mFHR-A, whose sequence is derived from the original characterization of class A mFHR transcripts. Following expression and purification of proteins using a 293-F mammalian expression system, functional assays were performed to understand how mFHR proteins modulate complement activation by competing with mFH for C3b/C3d on self-surfaces.

To assess the functional activity of recombinant mFH and mFHR proteins, different hemolytic assays were performed. Previous work has demonstrated that the last two SCR domains of FH (SCRs 19 and 20) are critical for FH-mediated protection of cell surfaces. To address whether the mFHR proteins deregulate mFH cell-surface protection, functional assays using mouse FH19–20 inhibitor, mFHR-A, mFHR-B, and mFHR-C were performed. In these hemolytic assays, normal sheep erythrocytes are added to complement sufficient wild-type mouse serum, but hemolysis of the cells is prevented by mFH that is present in the serum. Reduction of mFH from the surface of these cells results in AP activation and subsequent hemolysis. Here we were able to demonstrate that addition of mFHR-A and mFHR-B in the presence of normal mouse serum induced hemolysis of sheep erythrocytes. Both mFHR-A and mFHR-B act as potent antagonists of mFH on sheep erythrocyte cell surfaces. While the mFH19–20 inhibitor and mFHR-B induced ~50% hemolysis at ~7 μM concentration, mFHR-A is more potent and induced 100% hemolysis at ~2 μM. We also demonstrate that hemolysis can be prevented by addition of exogenous recombinant mFH to sheep erythrocytes prior to addition of mFHRs. Interestingly, mFHR-C does not appear to increase hemolysis of sheep erythrocytes but may exert effects on specific cell surfaces which has been suggested by other studies of mFHRs in different mouse models of autoimmune disease (26). Taken together, the results from hemolytic assays show that mFHR proteins are able to perturb the overall function of the alternative pathway. Furthermore, our results suggest that mFHRs may have different biological functions and/or recognize different surface ligands.

It should be noted that mFHR-A is a prototype for a protein encoded by the *mFHR-A* gene. A mRNA sequence isolated from a normal 5-month old mouse liver (BC026782) shares high homology to this prototype and can be found in the UCSC Genome Database, however evidence for a mFHR-A protein does not currently exist. Most interestingly is that the mFHR-A prototype, which shares >95% identity to mFHR-B SCRs 5–7 and 19–20, is a more potent inhibitor of FH than mFH19–20. The mFHR-A prototype contains two additional SCR domains corresponding to mFH SCRs 8–9 which may enable the protein to more efficiently compete with FH for binding to C3b on cell surfaces. The additional SCR domains within the mFHR-A and mFHR-B proteins may help them to engage GAG surfaces better than mFH19–20, thus making them more potent antagonists.

Additionally, our results with both mFHR-A and mFHR-B agree with functional studies of the human FHR proteins. Hemolytic assays with guinea pig erythrocytes show that both FHR-1 and FHR-5 inhibit FH function by competitively blocking the interaction between FH and C3b (11). Structural studies have established that this interaction occurs through FH SCRs19–20 and the reactive thioester containing domain (TED) located on the C3d part of C3b. Five residues (Asn1117, Asp1119, Gln1139, Tyr1142, and Tyr1190) within SCRs 19–20 form intermolecular hydrogen bonds with C3d. Sequence alignment of human FH and the mFH family shows that these residues are conserved between the two species. Therefore, we predicted that mFH and mFHRs would bind C3d and mutation of conserved residues within the binding interface would inactivate our proteins.

Apparent dissociation values for FHR-3 and FHR-4 were calculated as 87 nM and 260 nM respectively (27). They also demonstrated that FHR-3 and FHR-4 have similar binding affinities with C3b and that the reverse analysis, with FHRs immobilized on a chip and C3d/C3b in fluid phase, produced similar results. One caveat is that the kinetics of the human proteins were analyzed using a 1:1 binding model while the mouse proteins were fitted using a two-state reaction model. Taking this into consideration, the binding kinetics of mFHR-A and mFHR-B could also be compared to SPR results from the binding interaction observed between C3b and mutant human FHR-$5_{1212\text{-}9}$ protein (11, 28).

This mutant, found in patients with C3 glomerulopathy, has a duplicated dimerization domain (from duplication of SCRs 1–2). Binding affinities for wild-type mFHR-5 and mFH to amine couple C3b were determined to be 1.7 μM and 6.6 μM. While a binding affinity for the FHR-$5_{1212\text{-}9}$ mutant was not determined, functional analysis of this mutant using hemolytic assays also showed greater hemolysis than wild-type controls. This result was attributed to the mutant's increased ability to form higher order complexes and compete with FH for binding to C3b. Gel filtration chromatography (not shown) was used to analyze the native mFHR-B and results suggest that mFHR-B may be capable of forming higher order complexes. Given that the fit of both the mFHR-A and mFHR-B curves resembles the curve for FHR-$5_{1212\text{-}9}$, additional analysis of these proteins for the formation of higher-order complexes than dimers is necessary.

To further analyze the functional homology between the human and mouse C3d binding site, mutation of the putative C3d binding site on mFHR-A and mFHR-B was performed. Results show that mutation of two residues (corresponding to human FH residues N1117 and

Asp1119) was sufficient to disrupt mC3d binding of mFHR-A and mFHR-B in both ELISA and SPR assays. Additionally, Mutant mFHR-B exhibited significant loss of function in a sheep hemolytic assay further suggesting that mFHRs compete with mFH for the same target (C3b/C3d) on cell surfaces. The direct correlation between mFHR binding affinity for C3d and functional activity in hemolytic assays further establishes how these proteins modulate complement through competition with mFH for C3b/C3d on cell surfaces.

Additionally, the important role of other cell surface markers must also be addressed. The sheep hemolytic assay is dependent on FH recognition of C3b/C3d as well as sialic acid residues that are present on the cell surface. The ability of FH to engage C3b increases 10-fold in the presence of sialic acid residues and the structural basis for FH recognition of sialic acid on cell surfaces has been established (25). A recent study has proposed that FH simultaneously engages sialic acid and C3b in order to regulate complement activation (29). Mutation of sialic acid binding residues on FH19–20 resulted in the loss of its ability to antagonize FH. This suggests that the behavior of FH, and perhaps the ability of FHRs to antagonize FH function, is dependent on both C3b/C3d and surface sialic acid cell surface content. Implicit in this theory is that cells that possess low amounts of surface sialic acids (such as rabbit erythrocytes) are not subject to this same mechanism.

Understanding the behavior of FHRs on different cell-surfaces is critical for clarifying their associations with disease and explaining the different disease phenotypes. Here we also examined complement activation by mFHRs on two relevant cell lines. Our results showed increased C3b deposition on both murine tubular epithelial cells as well as normal human retinal pigment epithelial cells occurs when cells are incubated with normal mouse serum with addition of mFHR-A or mFHR-B. With both cell types, mFHR-A appears to generate greater complement activation than mFHR-B which supports our other binding and functional data. Additionally, complement activation by mFHRs on a human cell line and demonstration that mFHRs can bind human C3d, provides evidence that the murine proteins can serve as orthologs of human FHRs in animal studies. Together, these data provide important support for further evaluation of the roles of mFHRs *in vivo.*

While it is fairly straightforward to compare the sequence homology of C3b/C3d and GAG-binding sites between the different mFH and hFH protein families, it is much more challenging to make direct comparisons i.e. *does mFHR-B function more like human FHR-3 and FHR-4 or does it behave like FHR-5?* For direct comparisons such as this, better tools are required. Development of antibodies that recognize specific mFHR proteins is important for elucidating the different biological roles that these proteins may have and is currently being investigated. We have generated hamster anti-mouse monoclonal and polyclonal anti-FH and anti-FHR antibodies and observe bands that replicate original data by Hellwage et al. 2006 (10). While we attempted to generate monoclonal antibodies against recombinant mFHR-A and mFHR-B, we were not able to identify antibodies specific for mFHR-A and mFHR-B in WT or $FH^{-/-}$ mouse serum (Supplemental Fig. 3).

Finally, our results demonstrated that mFHR-C does not inhibit FH function in a sheep erythrocyte assay. These results suggest the possibility that mFHR-C has other important context-dependent biological functions. Compared to the mFHR-A and mFHR-B proteins,

mFHR-C contains twice as many SCR domains (14 SCRs), but is 6 SCR domains shorter than mFH. Notably, mFHR-C (as well as all other FHR proteins) lacks sequence homology to FH SCRs1–4, which are regulatory domains. Perhaps mFHR-C has a different role in cell-recognition and complement regulation? One could speculate that mFHR-C may have context-dependent functional roles, such in the kidney. Perhaps mFHR-C can destabilize C3 convertases on certain cell surfaces? Or maybe mFHR-C has fluid phase regulatory abilities and acts as a cofactor for FI? These results suggest that we must evaluate the mFHR proteins in a variety of different contexts in order to fully understand how they modulate complement. We must examine how FHRs regulate complement both in fluid phase versus on different cell surfaces taking into consideration that these proteins may function differently in the context of an autoimmune disease model versus a cancer or infectious disease animal model. Understanding the differences between mFHR-A/mFHR-B and mFHR-C may offer insight into how FHR proteins exert influence over complement regulation which could allow for strategic treatment against different diseases.

In summary, these results demonstrate that murine FHR proteins modulate complement activation by antagonizing FH function on cell-surfaces. Interestingly, we also show that neighboring genes, *mFHR-B* and *mFHR-C,* encode FHR proteins that have unique functions. While mFHR-B is a potent inhibitor of mFH, mFHR-C does not appear to have inhibitory functions which may be context dependent. Similar to human FHR-1 and FHR-5, mFHR-A or mFHR-B compete with mFH for binding to C3b/C3d on cell surfaces and have similar C3d binding affinities to FHR-3 and FHR-4. We identified that the binding interaction between C3d and mFHR proteins is conserved between human and murine systems. Furthermore, we demonstrate that mFHR binding affinities for C3d directly correlate with their functional activity in hemolytic assays. These results will be helpful for guiding future work in different animal models of disease, such as aHUS and AMD, which could potentially lead to the development of novel therapeutics.

Supplementary Material

Refer to Web version on PubMed Central for supplementary material.

Acknowledgments

This work was supported in part by a NIH R01 AR-51849, an investigator grant from the Beckman Institute for Macular Research (to V.M.H.), a University of Pennsylvania Health Systems Grant AI-18785 (to P.M.), a Victor W. Bolie and Earleen D. Bolie Graduate Scholarship (to A.H.A.), and the University of Colorado Cancer Core Protein Production Shared Resource, which receives direct funding support from the National Cancer Institute through the Cancer Center Support Grant (P30CA046934).

We would acknowledge Shaun Bevers for advice on circular dichroism experiments which were carried out at the Biophysics Core Facility, which is part of the Structural Biology and Biochemistry Department at the University of Colorado Anschutz Medical Campus. We would also like to thank Lori Sherman and Michelle Randolph for assistance with protein production.

References

1. Harboe M, Ulvund G, Vien L, Fung M, Mollnes TE. The quantitative role of alternative pathway amplification in classical pathway induced terminal complement activation. Clinical & Experimental Immunology. 2004; 138:439–446. [PubMed: 15544620]

2. Dragon-Durey MA. Heterozygous and Homozygous Factor H Deficiencies Associated with Hemolytic Uremic Syndrome or Membranoproliferative Glomerulonephritis: Report and Genetic Analysis of 16 Cases. J Am Soc Nephrol. 2004; 15:787–795. [PubMed: 14978182]

3. Levy M, Halbwachs-Mecarelli L, Gubler MC, Kohout G, Bensenouci A, Niaudet P, Hauptmann G, Lesavre P. H deficiency in two brothers with atypical dense intramembranous deposit disease. Kidney Int. 1986; 30:949–956. [PubMed: 2950269]

4. Richards A, Buddles MR, Donne RL, Kaplan BS, Kirk E, Venning MC, Tielemans CL, Goodship JA, Goodship THJ. Factor H Mutations in Hemolytic Uremic Syndrome Cluster in Exons 18–20, a Domain Important for Host Cell Recognition. The American Journal of Human Genetics. 2001; 68:485–490. [PubMed: 11170896]

5. Zhao J, Wu H, Khosravi M, Cui H, Qian X, Kelly JA, Kaufman KM, Langefeld CD, Williams AH, Comeau ME, Ziegler JT, Marion MC, Adler A, Glenn SB, Alarcón-Riquelme ME, Pons-Estel BA, Harley JB, Bae S-C, Bang S-Y, Cho S-K, Jacob CO, Vyse TJ, Niewold TB, Gaffney PM, Moser KL, Kimberly RP, Edberg JC, Brown EE, Alarcon GS, Petri MA, Ramsey-Goldman R, Vilá LM, Reveille JD, James JA, Gilkeson GS, Kamen DL, Freedman BI, Anaya J-M, Merrill JT, Criswell LA, Scofield RH, Stevens AM, Guthridge JM, Chang D-M, Song YW, Park JA, Lee EY, Boackle SA, Grossman JM, Hahn BH, Goodship THJ, Cantor RM, Yu C-Y, Shen N, Tsao BP. BIOLUPUS Network, GENLES Network. Association of genetic variants in complement factor H and factor H-related genes with systemic lupus erythematosus susceptibility. PLoS Genet. 2011; 7:e1002079. [PubMed: 21637784]

6. Prosser BE, Johnson S, Roversi P, Herbert AP, Blaum BS, Tyrrell J, Jowitt TA, Clark SJ, Tarelli E, Uhrín D, Barlow PN, Sim RB, Day AJ, Lea SM. Structural basis for complement factor H linked age-related macular degeneration. Journal of Experimental Medicine. 2007; 204:2277–2283. [PubMed: 17893204]

7. Zipfel, PF., Lauer, N., Skerka, C. Inflammation and Retinal Disease: Complement Biology and Pathology. Springer New York; New York, NY: 2010. The Role of Complement in AMD; p. 9-24.Advances in Experimental Medicine and Biology vol. 703

8. Vik DP, Keeney JB, MuñOz-Cánoves P, Chaplin DD, Tack BF. Structure of the murine complement factor H gene. Journal of Biological Chemistry. 1988; 263:16720–16724. [PubMed: 2972715]

9. Vik DP, MuñOz-Cánoves P, Kozono H, Martin LG, Tack BF, Chaplin DD. Identification and sequence analysis of four complement factor H-related transcripts in mouse liver. Journal of Biological Chemistry. 1990; 265:3193–3201. [PubMed: 1689298]

10. Hellwage J, Eberle F, Babuke T, Seeberger H, Richter H, Kunert A, Härtl A, Zipfel PF, Jokiranta TS, Józsi M. Two factor H-related proteins from the mouse: expression analysis and functional characterization. Immunogenetics. 2006; 58:883–893. [PubMed: 17028856]

11. Goicoechea de Jorge E, Caesar JJE, Malik TH, Patel M, Colledge M, Johnson S, Hakobyan S, Morgan BP, Harris CL, Pickering MC, Lea SM. Dimerization of complement factor H-related proteins modulates complement activation in vivo. Proc Natl Acad Sci USA. 2013; 110:4685–4690. [PubMed: 23487775]

12. Laskowski J, Renner B, Le Quintrec M, Panzer S, Hannan JP, Ljubanovic D, Ruseva MM, Borza D-B, Antonioli AH, Pickering MC, Holers VM, Thurman JM. Distinct roles for the complement regulators factor H and Crry in protection of the kidney from injury. Kidney Int. 2016

13. Morgan HP, Schmidt CQ, Guariento M, Blaum BS, Gillespie D, Herbert AP, Kavanagh D, Mertens HDT, Svergun DI, Johansson CM, Uhrín D, Barlow PN, Hannan JP. Structural basis for engagement by complement factor H of C3b on a self surface. Nature Structural & Molecular Biology. 2011; 18:463–470.

14. Ericsson UB, Hallberg BM, Detitta GT, Dekker N, Nordlund P. Thermofluor-based high-throughput stability optimization of proteins for structural studies. Anal Biochem. 2006; 357:289–298. [PubMed: 16962548]

15. Ferreira VP, Herbert AP, Hocking HG, Barlow PN, Pangburn MK. Critical role of the C-terminal domains of factor H in regulating complement activation at cell surfaces. The Journal of Immunology. 2006; 177:6308–6316. [PubMed: 17056561]

16. Thurman JM, Renner B, Kunchithapautham K, Ferreira VP, Pangburn MK, Ablonczy Z, Tomlinson S, Holers VM, Rohrer B. Oxidative stress renders retinal pigment epithelial cells susceptible to complement-mediated injury. J Biol Chem. 2009; 284:16939–16947. [PubMed: 19386604]

17. Renner B V, Ferreira P, Cortes C, Goldberg R, Ljubanovic D, Pangburn MK, Pickering MC, Tomlinson S, Holland-Neidermyer A, Strassheim D, Holers VM, Thurman JM. Binding of factor H to tubular epithelial cells limits interstitial complement activation in ischemic injury. Kidney Int. 2011; 80:165–173. [PubMed: 21544060]

18. Nagar B, Jones RG, Diefenbach RJ, Isenman DE, Rini JM. X-ray crystal structure of C3d: a C3 fragment and ligand for complement receptor 2. Science. 1998; 280:1277–1281. [PubMed: 9596584]

19. Cheng ZZ, Hellwage J, Seeberger H, Zipfel PF, Meri S, Jokiranta TS. Comparison of surface recognition and C3b binding properties of mouse and human complement factor H. Mol Immunol. 2006; 43:972–979. [PubMed: 16023208]

20. Kajander T, Lehtinen MJ, Hyvärinen S, Bhattacharjee A, Leung E, Isenman DE, Meri S, Goldman A, Jokiranta TS. Dual interaction of factor H with C3d and glycosaminoglycans in host-nonhost discrimination by complement. Proc Natl Acad Sci USA. 2011; 108:2897–2902. [PubMed: 21285368]

21. Renner B, Coleman K, Goldberg R, Amura C, Holland-Neidermyer A, Pierce K, Orth HN, Molina H, Ferreira VP, Cortes C, Pangburn MK, Holers VM, Thurman JM. The complement inhibitors Crry and factor H are critical for preventing autologous complement activation on renal tubular epithelial cells. J Immunol. 2010; 185:3086–3094. [PubMed: 20675597]

22. Thurman JM, Ljubanovic D, Royer PA, Kraus DM, Molina H, Barry NP, Proctor G, Levi M, Holers VM. Altered renal tubular expression of the complement inhibitor Crry permits complement activation after ischemia/reperfusion. J Clin Invest. 2006; 116:357–368. [PubMed: 16444293]

23. Blackmore TK, Sadlon TA, Ward HM, Lublin DM, Gordon DL. Identification of a heparin binding domain in the seventh short consensus repeat of complement factor H. J Immunol. 1996; 157:5422–5427. [PubMed: 8955190]

24. Blackmore TK, Hellwage J, Sadlon TA, Higgs N, Zipfel PF, Ward HM, Gordon DL. Identification of the second heparin-binding domain in human complement factor H. J Immunol. 1998; 160:3342–3348. [PubMed: 9531293]

25. Blaum BS, Hannan JP, Herbert AP, Kavanagh D, Uhrín D, Stehle T. Structural basis for sialic acid-mediated self-recognition by complement factor H. Nat Chem Biol. 2015; 11:77–82. [PubMed: 25402769]

26. Mehta G V, Ferreira P, Skerka C, Zipfel PF, Banda NK. New insights into disease-specific absence of complement factor H related protein C in mouse models of spontaneous autoimmune diseases. Mol Immunol. 2014; 62:235–248. [PubMed: 25033230]

27. Hellwage J, Jokiranta TS, Koistinen V, Vaarala O, Meri S, Zipfel PF. Functional properties of complement factor H-related proteins FHR-3 and FHR-4: binding to the C3d region of C3b and differential regulation by heparin. FEBS Letters. 1999; 462:345–352. [PubMed: 10622723]

28. Tortajada A, Yébenes H, Abarrategui-Garrido C, Anter J, García-Fernández JM, Martínez-Barricarte R, Alba-Domínguez M, Malik TH, Bedoya R, Cabrera Pérez R, López Trascasa M, Pickering MC, Harris CL, Sánchez-Corral P, Llorca O, Rodríguez de Córdoba S. C3 glomerulopathy-associated CFHR1 mutation alters FHR oligomerization and complement regulation. J Clin Invest. 2013; 123:2434–2446. [PubMed: 23728178]

29. Hyvärinen S, Meri S, Jokiranta TS. Disturbed sialic acid recognition on endothelial cells and platelets in complement attack causes atypical hemolytic uremic syndrome. Blood. 2016; 127:2701–2710. [PubMed: 27006390]

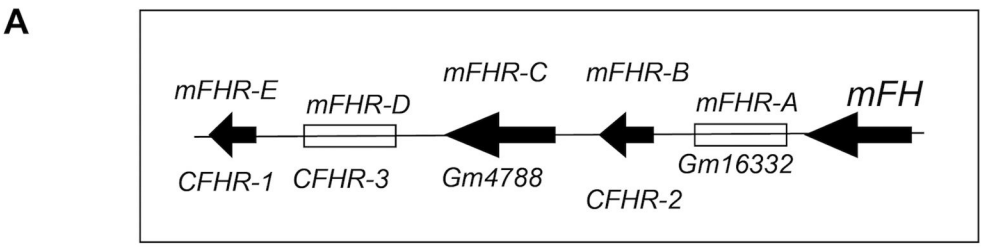

Gene Name:	Mouse Chromosome 1 Location (Ensembl.org)
mFH	140,085,859-140,183,411
mFHR-A	139,862,957-139,936,477
mFHR-B	139,810,288-139,858,702
mFHR-C	139,697,623-139,781,243
mFHR-D	139,584,783-139,660,899
mFHR-E	139,547,053-139,560,272

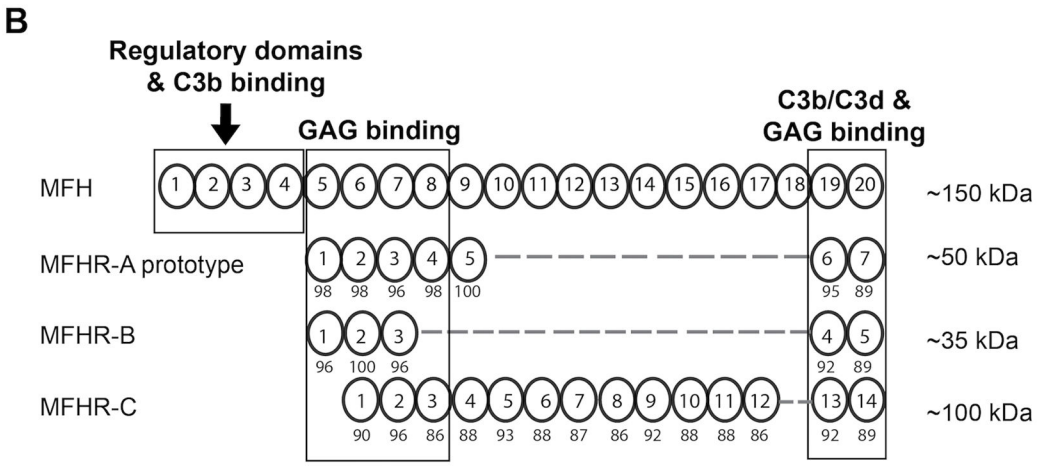

Figure 1. Mouse FH and FHR gene family and schematic representation of recombinant mFH and mFHR proteins

A) Representation of *mFH* and *mFHR* genes and their locations on mouse chromosome 1. Boxed regions indicate genes listed by some databases as unprocessed pseudogenes. **B)** Similar to human FH, mFH has 20 SCR domains. The first four domains are involved in regulation and C3b binding. The next four domains are involved in glycosaminoglycan (GAGs) binding and the last two domains are involved in C3b/C3d and GAG binding. Two of the mouse FHR proteins, mFHR-B and mFHR-C, have been previously described. The mFHR-A prototype is designed based on a sequence described by Vik et al. 1990. The mFHR proteins A–C are shown with their SCR domains (numbered inside each circle) aligned with SCR domains of mFH (with percentage homology with mFH shown below each SCR).

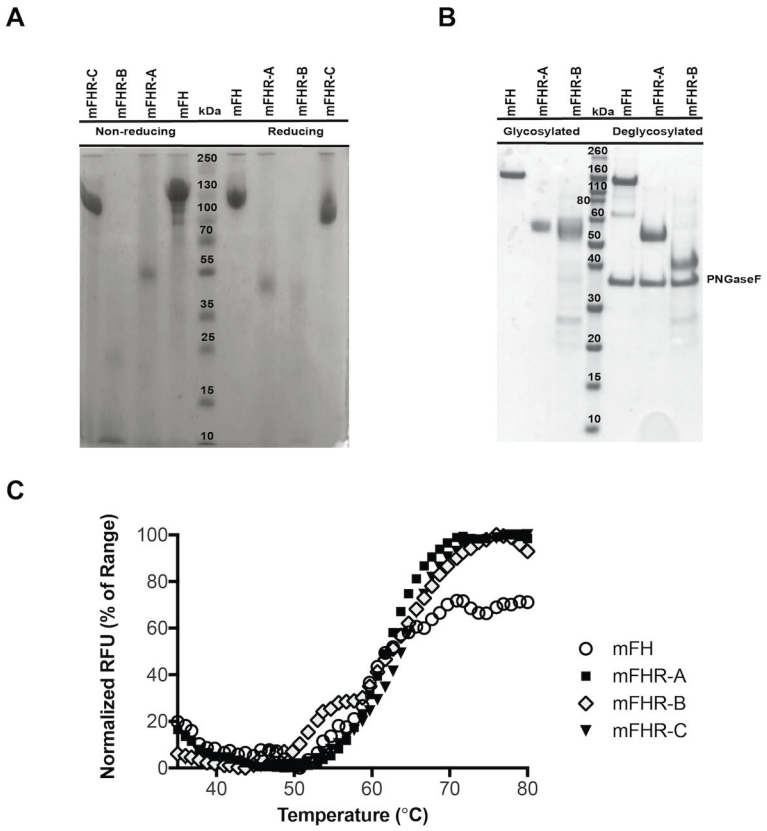

Figure 2. Recombinant mFH and mFHR analysis

A) SDS-PAGE analysis of recombinant mFH and mFHR proteins under reducing conditions on a 12% Bis-Tris gel. Approximately 2 μg of each protein was loaded per well with masses indicated using a PageRuler Plus Ladder. Proteins are shown both glycosylated and deglycosylated. The PNGaseF enzyme was removed from these deglycosylated samples. B) Comparison of deglycosylated mFHR-A and mFHR-B proteins using 12% SDS-PAGE analysis and a Novex Sharp Protein Ladder. PNGaseF has a molecular weight of ~36kDa and is marked by an arrow. C) Thermal melting (T_m) profiles of mFH (circle), mFHR-A (square), mFHR-B (star), and mFHR-C (hexagon). Normalization of the RFU values for each protein was performed for a better visual comparison among the different proteins. All mFH and mFHR proteins have a T_m between 60–65°C. The data represent normalized RFU values from three separate experiments.

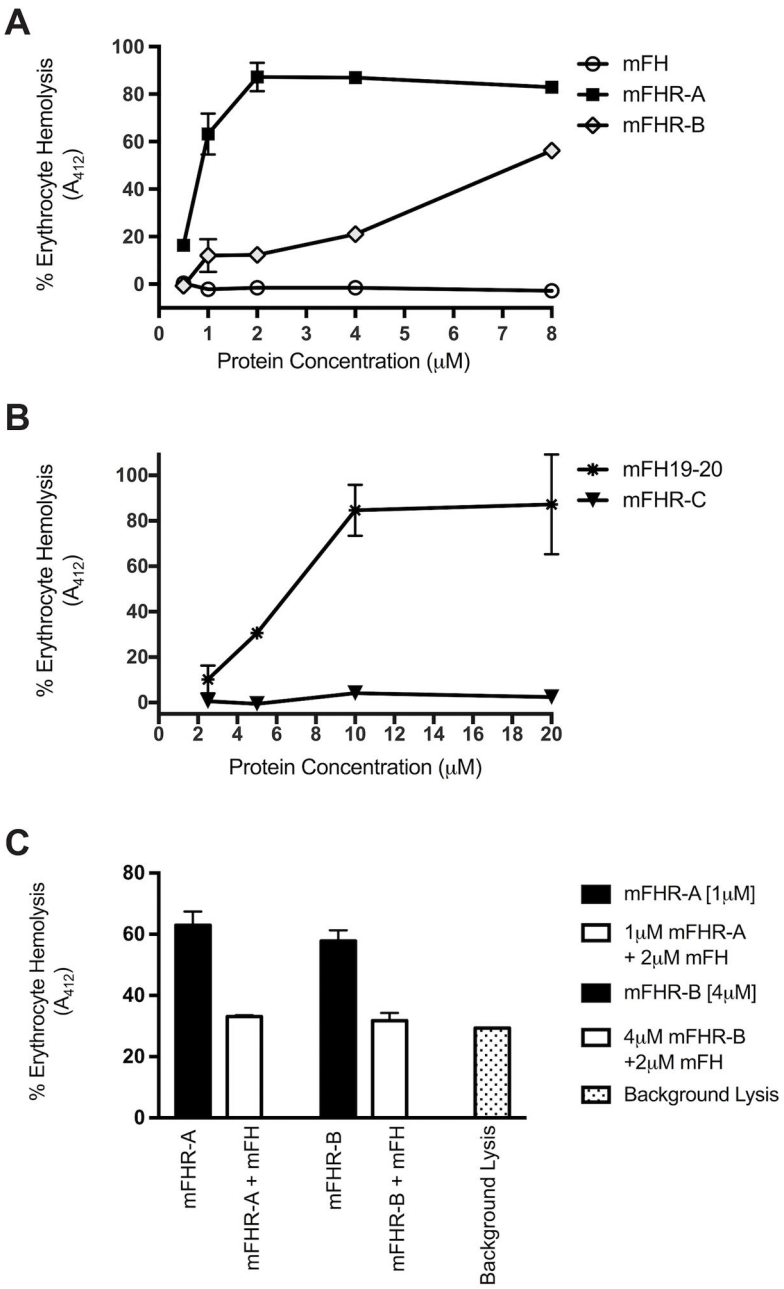

Figure 3. Mouse FHR-A and FHR-B are potent antagonists of FH on host-like surfaces

Hemolysis assays were performed using 1×10^6 sheep erythrocytes in a 24 μL reaction volume with 40% normal mouse serum. Hemolysis was determined after incubation of the reaction for 30 min at 37°C followed by quenching with GVBE and measurement of the absorbance at 412 nm. A) mFHR-A (square) is a more potent inhibitor of mFH (open circle) than mFHR-B (open diamond). Nearly 100% lysis is observed with less than 4 μM mFHR-A, while mFHR-B requires two fold more protein to induce just over 50% lysis of erythrocytes. B) mFH19–20 (star) is a previously characterized inhibitor of murine FH. This inhibitor, which is comprised of mFH SCRs 19–20, competes with the C-terminal end of FH

for binding to C3b and polyanionic rich surfaces. mFHR-C (closed triangle) does not antagonize mFH function including at 20 μM concentration. C) Competition hemolytic assay using mouse FH. Incubation on ice of 2μM of recombinant mouse FH to 1×10^6 sheep erythrocytes in a 24 μL reaction volume with 20% normal mouse serum was performed prior to adding either 1μM mFHR-A or 4μM mFHR-B to the samples. Hemolysis was determined as described in Fig 3A. All data represent means ± SEM from at least three separate experiments with three replicates per sample.

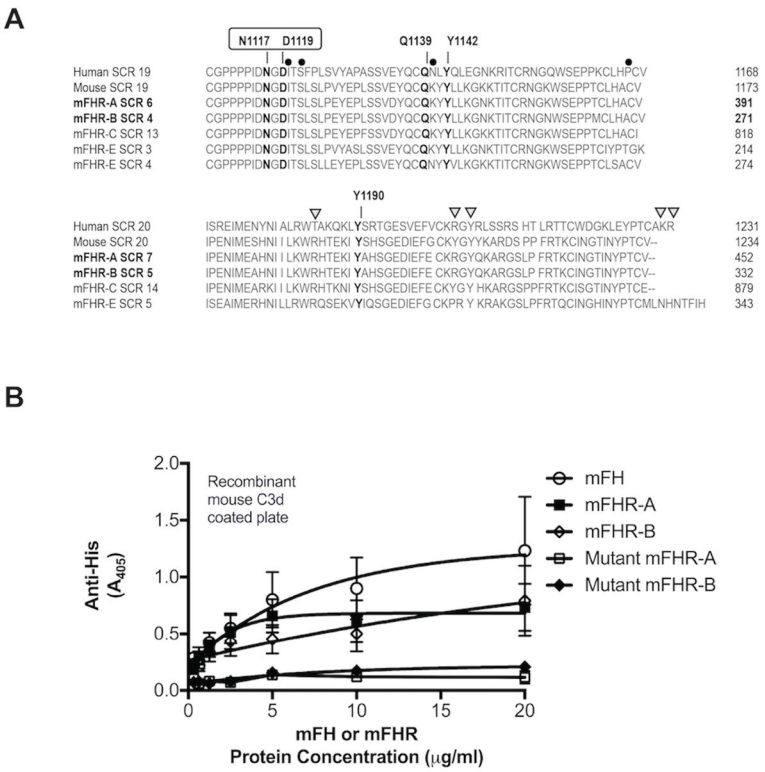

Figure 4. Human FH SCRs 19–20 aligned with mFH and mFHR proteins showing putative C3d binding sites

A) Alignment of human FH (hFH) SCRs 19 and 20 with corresponding mouse SCR domains of mFH (Uniprot: P06909), mFHR-A (prototype sequence for mFHR-A based on Vik et al. clone 3A4/5G4 Uniprot: Q61407), mFHR-B (Uniprot: Q4LDF6), mFHR-C (Uniprot: Q0KHD3) and mFHR-E (Uniprot: Q61406). Residues marked in bold have side chains which form hydrogen bonds with C3d. Mutations N1117A and D1119 (circled) were made at corresponding positions on mFHR-A and mFHR-B to create mutant constructs used in ELISA and surface plasmon resonance assays. Residues marked by a circle are part of the interface between hFH19–20:C3d, yet are not found in all of the mouse FH and FHR proteins. The residues marked by a triangle have been indicated in an additional proposed FH: C3d interaction, yet are not entirely conserved within the mouse FH and FHR family. mFHR-E has two SCR domains (SCRs 3 and 4) which share high sequence identity to hFH and mFH SCR 19. The mFHR-D gene is also listed in various databases as an unprocessed pseudogene, and is not depicted here. B) Mouse FH and mFHRs bind mC3d but mutant proteins are inactive. ELISA analysis of plate-bound mC3d with mFH, mFHR-A, and mFHR-B. Residues on human FH SCR19 which contribute to side-chain interactions with C3d are conserved in mFHR-A and mFHR-B. Mutation of two residues was performed (corresponding to human FH residues N1117A and D1119A) and no binding was observed for the mutant mFHR-A and mFHR-B proteins. The data represent means ± SEM from at least three separate experiments.

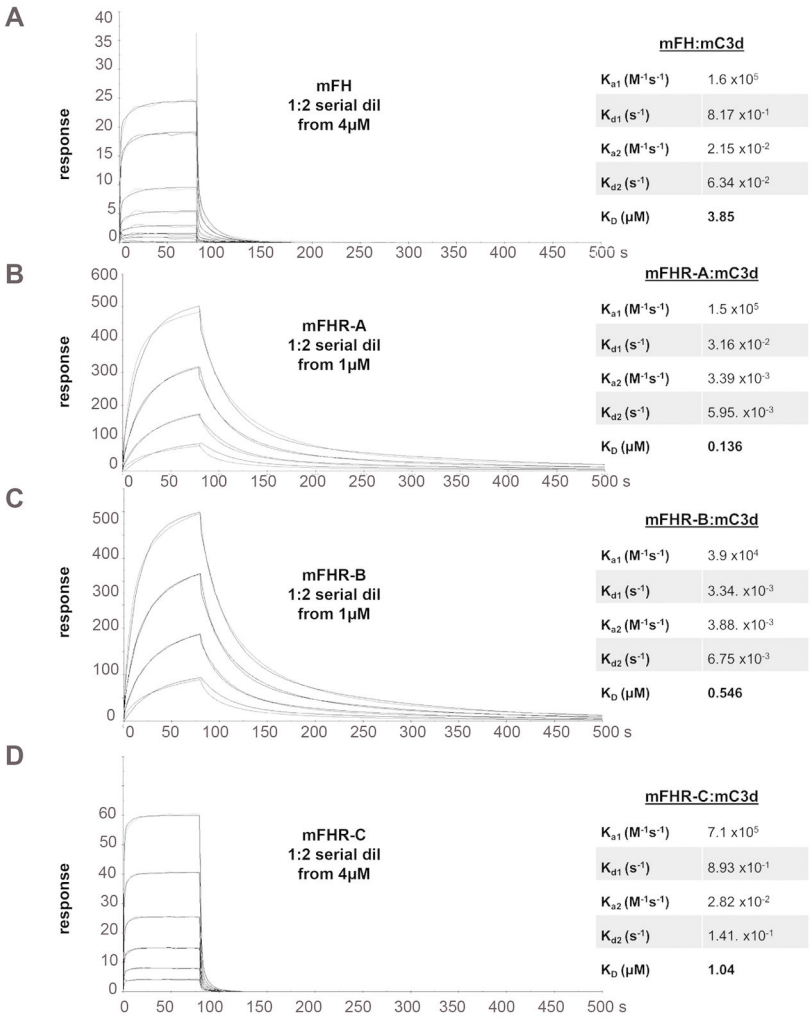

Figure 5. Binding of mouse C3d and mFH and mFHR proteins. Surface plasmon resonance was used to analyze the binding between mouse C3d and mFH and mFHR proteins

Serial dilutions (1:2) of mFH starting at 4 μM (A), mFHR-A starting at 1 μM (B), mFHR-B starting at 1 μM (C), and mFHR-C starting at 4 μM (D) were flowed over ~2500 resonance units of immobilized mC3d. Affinity values (K_D) were determined by fitting data to a two-state reaction model. Different binding kinetics were observed for mFHR-A and mFHR-B compared to mFH and mFHR-C and are displayed in the corresponding tables. Mutant mFHR-A and mutant mFHR-B did not bind mC3d either on ELISA (Fig. 4B) or using SPR.

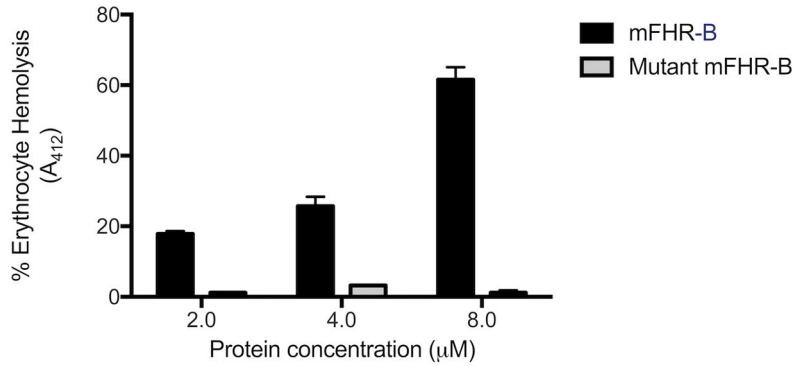

Figure 6. Mutant mFHR-B is inactive in sheep hemolytic assay

Mutation of two key mC3d binding residues (which correspond to human FH residues N1117A and D1119A) on wild-type mFHR-B greatly diminishes the ability of this protein to antagonize mFH function. The data represent means ± SEM from three separate experiments.

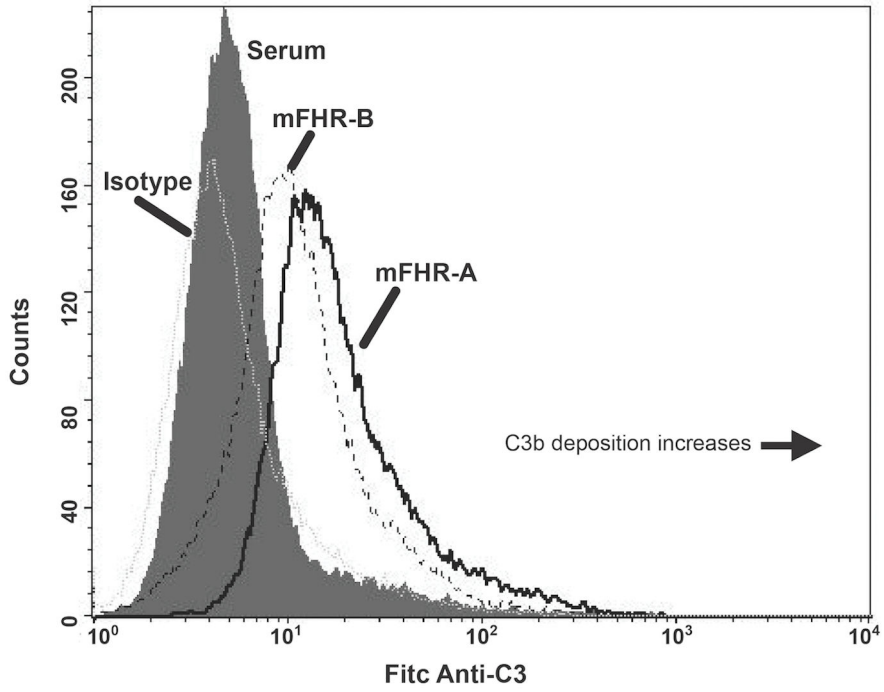

Figure 7. Mouse FHR-A and FHR-B are potent mFH antagonists on murine tubular epithelial cells (TECs)

Increased complement activation is observed, as indicated by C3b deposition, when mFHR-A and mFHR-B proteins are incubated with TEC cells in the presence of 10% normal mouse serum. Data are shown as a histogram that is representative of one of two separate experiments.

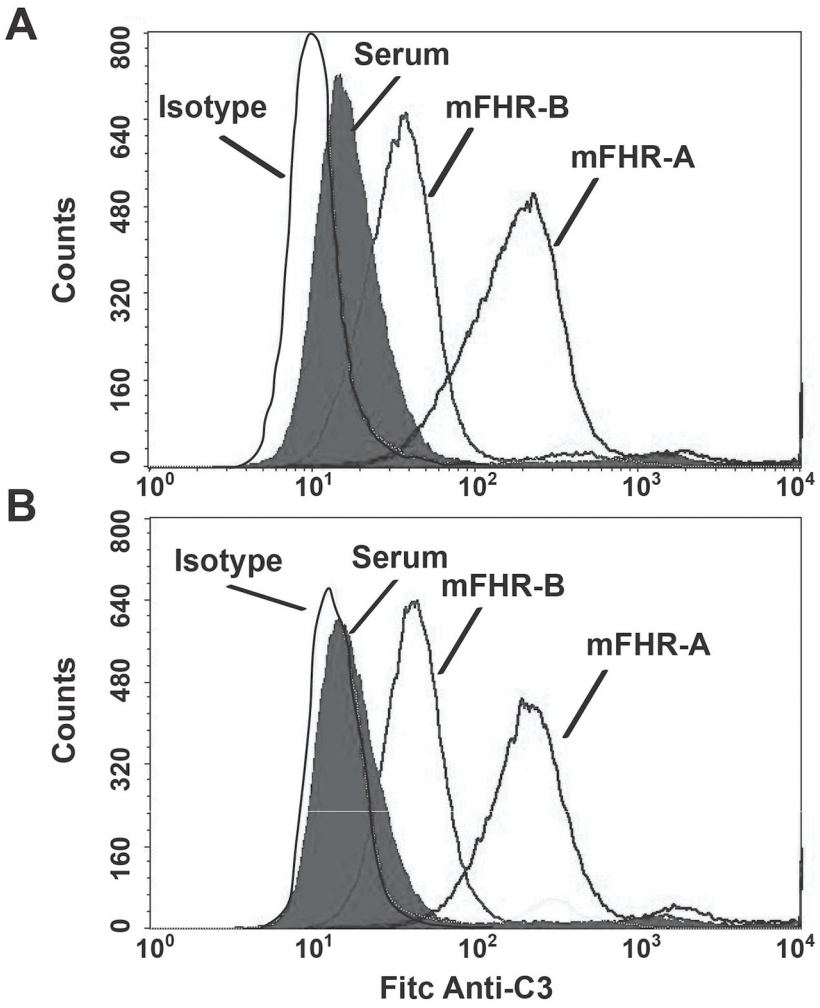

Figure 8. Both mFHR-A and mFHR-B increase complement activation on human retinal pigment epithelial cells (ARPE-19)

Incubation of mFHR-A and mFHR-B with ARPE-19 cells in the presence of 10% normal mouse serum induces C3b deposition on the surface of A) ARPE-19 cells stressed with H_2O_2 and B) unstressed ARPE-19 cells show increased C3b deposition after incubation with mFHR-A and mFHR-B proteins. Data are shown as a histogram that is representative of one of three experiments.